Automated screening of AURKA activity based on a genetically encoded FRET biosensor using fluorescence lifetime imaging microscopy

Florian Sizaire, Gilles Le Marchand, Jacques Pécréaux, Otmane Bouchareb, Marc Tramier

Automated screening of AURKA activity based on a genetically encoded FRET biosensor using Fluorescence Lifetime Imaging Microscopy

Florian Sizaire[1], Gilles Le Marchand[1], Jacques Pécréaux[1], Otmane Bouchareb[2] and Marc Tramier[1, 3*].

[1] Univ Rennes, CNRS, IGDR (Genetics and Development Institute of Rennes), UMR 6290, F-35000 Rennes, France
[2] Inscoper F-35510 Cesson-Sévigné, France
[3] Univ Rennes, BIOSIT, UMS CNRS 3480, US INSERM 018, F-35000 Rennes, France
* Correspondence and requests for materials should be addressed to M.T. (Genetics and Development Institute of Rennes (IGDR), 2 avenue du Prof. Léon Bernard, 35043 Rennes, France; +33223235487; marc.tramier@univ-rennes1.fr)

Abstract

Fluorescence Lifetime Imaging Microscopy (FLIM) is a robust tool to measure Förster Resonance Energy Transfer (FRET) between two fluorescent proteins, mainly when using genetically-encoded FRET biosensors. It is then possible to monitor biological processes such as kinase activity with a good spatiotemporal resolution and accuracy. Therefore, it is of interest to improve this methodology for future high content screening purposes. We here implement a time-gated FLIM microscope that can image and quantify fluorescence lifetime with a higher speed than conventional techniques such as Time-Correlated Single Photon Counting (TCSPC). We then improve our system to perform automatic screen analysis in a 96-well plate format. Moreover, we use a FRET biosensor of AURKA activity, a mitotic kinase involved in several epithelial cancers. Our results show that our system is suitable to measure FRET within our biosensor paving the way to the screening of novel compounds, potentially allowing to find new inhibitors of AURKA activity.

Keywords: fluorescence lifetime, FRET biosensor, screening, AURKA

Introduction

Since several years, FLIM has been widely used to measure the fluorescence lifetime of fluorescent proteins (Becker, 2012). It is an intrinsic parameter independent of concentration, which, however, depends on the environment of the fluorophore such as FRET, a non-radiative energy transfer from excited fluorescent donor dipole to a close acceptor dipole (<10nm). Given that, a decrease of the donor fluorescence lifetime is observed when FRET is present (Lakowicz, 2006) and lifetime is often used as a way to measure FRET. In this light, FRET-FLIM has been

widely used to investigate protein-protein interactions (Kenworthy, 2001; Padilla-Parra and Tramier, 2012), cleavage activity of proteases (Horton et al., 2007), protein oligomerization (Richert et al., 2015). Originally developed for calcium signalling (Miyawaki et al., 1997), genetically encoded-FRET biosensors have opened new perspectives in quantitative fluorescence microscopy. These biosensors are now powerful tools to investigate biological events in living cells (Hochreiter et al., 2015). In addition, the development of kinase FRET biosensors allowed to track the activity of kinases within living cells in time and space (Sizaire and Tramier, 2017; Zhang et al., 2001). High-content screening (HCS) is a widespread methodology to screen and design new inhibitors and it can be adapted to microscopy setups (Thomas, 2010). Different systems combining screening with FRET-FLIM have arisen allowing to study protein-protein interaction (Guzmán et al., 2016; Margineanu et al., 2016) or to find new epigenetics markers in cancer (Liu et al., 2019). More recently, screening combination with FRET-FLIM seems to be a new promising methodology for pharmacological screenings (Guo et al., 2019). In this article, we present a novel pipeline, consisting of an automated FRET-FLIM microscope used to screen AURKA activity with a FRET biosensor. AURKA is a serine/threonine kinase and has been first described as a mitotic kinase in Drosophila (Glover et al., 1995). It plays several roles in cell division such as mitotic entry, maturation of centrosomes, assembly of the mitotic spindle and the midbody (Nikonova et al., 2013). AURKA is known to be an oncogene and is overexpressed in several epithelial cancers (Bischoff et al., 1998; Sen et al., 1997). Our team has developed a genetically encoded FRET biosensor of AURKA which consists of the whole kinase flanked by the GFP and mCherry fluorophores (Bertolin et al., 2016). We showed that the conformational change of the kinase, which is indicative of its activation, modifies the proximity between GFP and mCherry increasing FRET efficiency. This biosensor has been validated to be a suitable tool to find new non-mitotic roles of the kinase, particularly at mitochondria to control organelle dynamics and energy production (Bertolin et al., 2018). Thereby, in collaboration with Inscoper (www.inscoper.com), we have developed the control solution of our time-gated FLIM microscope (fastFLIM) (Leray et al. 2013). Finally, we present the optimization of this system to screen a 96-well plate with cells expressing the AURKA biosensor, together with the automated process to analyse data.

Material and Methods

Cell culture

U2OS cells free from mycoplasma were purchased from American Type Culture Collection (ATCC, HTB-96) and were grown in Dulbecco's modified Eagle's medium (DMEM, Sigma-Aldrich) supplemented with 10% fetal bovine serum (Life Technologies, Thermo Fisher Scientific), 1% L-glutamine (Life Technologies, Thermo Fisher Scientific) and 1% penicillin–streptomycin (Life Technologies, Thermo Fisher Scientific). Cells were cultivated at 37°C and 5% CO_2. The generation of GFP-AURKA and GFP-AURKA-mCherry stable cell lines were generated by transfecting U2OS cells with X-tremeGENE HP transfection reagent (Roche), following the manufacturer's indications. Stable clones were selected in DMEM supplemented with 10% fetal bovine serum, 1% L-glutamine, 1% penicillin–streptomycin and 500 µg/ml Geneticin (Invivogen). Stable and transient transfections were performed with X-tremeGENE HP transfection reagent (Roche) according to the manufacturer's instructions.

Cell preparation for microscopy

Mitotic cells were obtained after synchronisation at the G2/M transition with 100 ng/ml nocodazole (Sigma-Aldrich) for 16h at 37°C. Cells were washed twice with 1X PBS and incubated with prewarmed medium for 30 min to reach metaphase. For inhibitor screening, 47 molecules provided by KISSf (Roscoff) were used. Each molecule was used as duplicate in a 96-well plate and cells were blindly incubated with molecules at 1 µM for 30 minutes at 37°C. Cells were washed with PBS 1 X and were fixed with paraformaldehyde 4% (from paraformaldehyde 16% (Electron Microscopy Sciences), diluted in PBS) for 15min at room temperature. Cells were washed three times with 1X PBS and were kept in PBS at 4°C or directly used for microscopy. All microscopy experiments were performed in Nunc Lab-Tek II Chamber slides (Thermo Fisher Scientific) or in 96-well plate glass cover (Zell-kontak).

FLIM microscopy

The fastFLIM microscope is presented in details in Results section. Briefly, the time-gated FLIM system is constituted of a White light laser (Fianium sc400) and an home-made wavelength selector for excitation source, a spinning disk microscope with Yokogawa confocal head (CSU X1) and Leica microscope (DMI8) with 20x Leica water immersion (NA = 0.7), and a fast time-gated intensifier (Picostar Lavision using Kentech instrument HRI) optically coupled to a CCD camera (Coolsnap HQ Photometrics) for wide-field detection. The system is

completely controlled by Inscoper hardware and software solution in order to provide HCS-FLIM protocols for screen acquisitions.

Data and statistical analysis

Home-made automated protocol was used for lifetime calculation and cell segmentation using ImageJ macro (see details in Results section). The code is available through github at https://github.com/FloIGDR/Macro-ImageJ/blob/master/Screening%20analysis.
The Mann-Whitney test was used to compare the fluorescence lifetime between GFP-AURKA and GFP-AURKA-mCherry (Fig 1.C, Fig 5.A).

Results and discussion

Time-gated FLIM microscopy for fast cellular measurements of the AURKA FRET biosensor in a large field of view

We previously described our microscope setup for rapid FLIM acquisition (the fastFLIM microscope) (Leray et al., 2013). This system can image and measure the fluorescence lifetime of any fluorescent protein with a high frame rate in comparison to conventional techniques such as TCSPC. Besides, based on a new method for controlling a plurality of functional modules (Roul et al., 2015), the Inscoper company has recently developed a control solution for microscopy systems used in life science. The solution includes an electronic device embedding a microcontroller to autonomously execute sequences of microscope driving commands and an application software offering the human-machine interface. The advantages of this solution are the user-friendly interface and significantly increased acquisition speeds. To further increase the speed capabilities of the fastFLIM microscope, we have developed an implementation of the Inscoper control system to be conjugated with the microscopy setup. The system is represented in Fig. 1A. Before the acquisition, the Inscoper device receives the commands sent by the user through the computer and will then drive autonomously and directly all the devices during acquisition. The microscopy setup works using the visible spectrum of a supercontinuum pulsed laser source with a frequency of 40 MHz (Fianium sc400) and filtered by a home-made wavelength selector to choose any band between 420 nm and 700 nm as light excitation. This latter goes through a spinning disk microscope (Yokogawa CSU X1 and Leica DMI8 microscope) that allows us to perform confocal microscopy in wide-field detection mode and then reaches the sample. The fluorescence emission light, after passing through the dichroic and the emission filter, goes through a fast time-gated intensifier (Picostar Lavision integrating an HRI Kentech Instrument). The intensifier temporal gates of 2.2 ns is triggered by the

excitation pulse signal coming from the laser. A delay generator on the trigger signal is used to shift the gate. The time-gated wide-field fluorescence image is then captured by a CCD camera (Coolsnap HQ Photometrics) and further sent to the computer. During the acquisition process, on top of the spinning disk, the microscope status, and the CCD camera, the Inscoper box drives the delay generator to produce different time-gated images. When using GFP fluorescence, whose lifetime is around 2.5 ns, we performed five time-gated images of 2.2 ns with a consecutive shift of 2.2 ns to produce adjacent temporal gates (Fig. 1B). The stack of five time-gated images covers the whole fluorescence decay of the GFP. From the intensity of these images, using a discrete equation to compute the temporal mean, the computer gets the mean fluorescence lifetime pixel by pixel, and ultimately the FLIM image. The strength of this approach lies in getting rid of fitting methods, allowing reduced photon budget (Leray et al., 2013). The application software then displays the FLIM image in real time for easy-to-use experiments.

We have recently designed a FRET-based biosensor for AURKA that allows us to track AURKA activation in living cells (Bertolin et al., 2016). This biosensor is composed of the whole kinase flanked by a GFP and a mCherry (hereby GFP-AurkA-mCherry) and is stably expressed at physiological levels in U2OS cells. In these cells, GFP-AUKA-mCherry shows a decrease in GFP lifetime of nearly 100 ps compared to the donor alone (GFP-AURKA). This decrease in lifetime is indicative of FRET, and we have shown that this 100 ps downshift corresponds to the difference between activated or inactivated kinase. The use of this biosensor has been validated in living cells using a 63x objective with oil immersion and high numerical aperture to image one single cell per image. However, this approach is not suitable for the screening of AURKA activation in 96-well plates, as mitosis in these cells occurs every 24h and it lasts for 1h30 only. Thus, we have decided to switch from live cells to fixed cells to overcome this issue. We synchronized these cells at mitosis, and we fixed them using paraformaldehyde. We then changed the objective from a 63x oil immersion to a 20x water immersion (NA = 0.7) in order to image several mitotic cells in every field of view (Fig. 1C). Concerning the biological sample, we verified that the fixation does not abolish FRET detection. On fixed cells, we measured a difference of 100 ps between GFP-AURKA and GFP-AURKA-mCherry, which corresponds to the FRET previously observed in living cells either with the fast-FLIM or by Time-Correlated Single Photon Couting (TCSPC). Together, we are able to use fast acquisition of FRET-FLIM images in a large field of view. This allows to

increase the number of the mitotic cells detected per acquisition and without losing FRET efficiency although we lose some spatial resolution.

Inscoper: an embedded control software for fast acquisition in fluorescence microscopy

The Inscoper imaging suite was grounded on separating the microscope and associated devices control from the user interface (Fig.2). The Inscoper electronic unit performs the control of all the devices around the microscope during the image acquisition. Thus, for the fast FLIM system, the Inscoper box ensures bidirectional communication with all motorised devices. In contrast, the Inscoper interface, run on a PC, is only used to set up the acquisition, to retrieve the images from the camera and later to visualize them. The Inscoper box offers the advantage of running the driving sequence, customised to the very experiment, without an operating system and this avoids in particular reliability issue related, e.g. to OS update as often found when using conventional acquisition software. Furthermore, since the driving code is embedded on a microcontroller, it performs in real time. Overall, it allows rapid and stable communication with the devices keeping full synchronisation of all the signals and ensures highly reproducible experiments. The Inscoper interface gives the user access to many settings for multidimensional experiments, such as timelapse, multi-channel, Z-series and multi-positions ones. Regarding the fastFLIM, when the user starts a FLIM acquisition, the Inscoper box controls the illumination system, the focus of the microscope, the delay generator to select the shift of the delay gate at 2.2 ns, and the stage for each new XY position. These parameters can be manually adjusted when the user starts a new FLIM acquisition. Among the parameters controlled by the Inscoper box, only the image data goes directly to the computer from the camera. Furthermore, the Inscoper box uses a bidirectional communication with the camera based on multiple trigger signals. Doing so, we tightly synchronize the camera frame grabbing and the configuration changes of the microscope and associated devices. In particular, before sending the trigger to the camera to grab a new image, the Inscoper box waits for a trigger ready signals from the camera and « new configuration reached » from the devices. A third signal called *exposure out* notify the other devices that the camera is in readout step.

Automatised screening coupled with autofocus to acquire mitotic cells expressing the AURKA FRET biosensor within a 96-well plate

We aim to perform an automated screening on a 96-well plate using the fastFLIM microscope. We have developed the necessary plugins within the Inscoper microscope-control application to overcome issues cause by screening methodology (Fig. 3A). They include a randomised

multi-position mode for each independent well, and autofocus. The design of the software interface is presented in Fig. 3B. Given that the fastFLIM microscope stage is motorized and controlled by the Inscoper box, the features of a 96-well plate such as the length, the width, the size of the well and the distance between the wells were uploaded to allow the stage to automatically browse the entire plate for the multi-position mode. The user can then choose to screen the entire plate or definite number of wells. In addition, the user can also choose to image multiple positions in each well. The positions within the different wells are randomly determined to up to hundreds of positions for each well. In order to avoid overlap of the different fields of view, a minimal distance between each position can be defined. For example, using the 20x objective, we determined a minimal distance of 250 µm between each position which corresponds to the size of the field of view, and we set this parameter directly in the interface. After defining the above-mentioned parameters, all the positions for every selected well of the 96-well plate are calculated to use the Inscoper solution as for conventional multi-position imaging. Concerning autofocus, it addresses a major challenge when screening long distance multi-position in cellular microscopy. Although manufacturers develop the flattest plates possible, a slight variation of a few µm between wells exists and leads to a focus loss. Furthermore, depending on the application, the focus of interest (z position of the cell) can be different from well to well. To overcome this issue, several strategies exist (Qiu et al., 2013). We adapted an autofocus method based on the analysis of sharpness on a z-stack of images. In further details, the user chooses the number and the size of the z-steps being analysed. For each step, an image of fluorescence intensity is acquired and a 3x3 median filter is applied. Then, a sharpness score is calculated for each pixel, and an additive sharpness score is determined for the image. This score is used to determine the z-position of the best focus. Different channels can be used for acquisition and autofocus so that any excitation lights and cell labelling can be used. This also enables the user to avoid photobleaching and phototoxic effect related to the labelling used for the FLIM. In the experiment presented here, we observed that with a minimum illumination of GFP, we were still able to find the best focal plane of cells expressing GFP-AURKA and GFP-AURKA-mCherry and this without perturbing the GFP fluorescence lifetime. This is why we decided to use the GFP illumination for the autofocus procedure as well.

An automatized data analysis pipeline for screening: cell-by-cell fluorescence lifetime determination

Depending on the number of positions for each well, the number of images can vary from hundreds to thousands, calling for automatically analysing the data. Since a single frame contains multiple cells, we segmented the image to compute cell-wise measurements later. Our data analysis pipeline (Fig. 4) stores the time-gated stack of fluorescence images, the corresponding fluorescence lifetime images, and the cropped images of segmented cells together with a table summarizing the available measurements for this cell. At first, we compute the FLIM images in a post-acquisition step. The advantage is to adjust the parameters along the process and have the ability to recompute the mean lifetime posteriorly, an important feature to tweak, e.g. the pixel threshold value of the first time-gated image. Indeed, this latter value limits the extent of the fluorescence lifetime computing, as pixels below the threshold do not have sufficient photon count to let us compute a reliable lifetime. In our case, a threshold at 3000 grey levels appears suitable (Leray et al., 2013). The computing is performed by an *ad hoc* ImageJ macro in which the user is asked to provide the size of the intensifier gate (gatewidth), the step between the different time-gated images (stepdelay) and the threshold value (grey value). In a second step, we segment the cells using the first time-gated intensity image, which harbours the highest intensities. To do so, we performed a Gaussian blur, followed by an automatic threshold in ImageJ. The corresponding parameter and threshold-determining algorithm are set by the user prior to batch processing. In our case of cells expressing the AURKA biosensor and synchronized at mitosis, a Gaussian blur provided by ImageJ using a 1-pixel radius circular neighbourhood and the default threshold-determining algorithm offer the highest accuracy possible. Finally, the watershed algorithm separates adjacent cells. Different regions of interest are then determined. The lifetime image is then broken into cropped sub-frames containing each a single cell and saved in separated files together with a file indicating the mean fluorescence lifetime over the cell, the standard deviation and cell-area in pixels. It allows controlling the quality of the segmentation and further statistical analyses.

Validation of a 96-well plate screening using AURKA FRET biosensor

To validate our screening process, we investigated a 96-well plate containing U2OS stable cell lines expressing GFP-AURKA or GFP-AURKA-mcherry (Fig. 5). We seeded the same amount of cells in each well and synchronised them in mitosis using nocodazole. This is known to induce a peak of AURKA expression (Nikonova et al., 2013) and correspondingly a peak of signal from the biosensor. Then, cells were released in normal medium for 30 min and reach

metaphase. The use of a multi-channel pipette allowed a homogenous synchronization throughout the 96 wells of the plate, and it ensured a rapid washout of the culture media in all the wells in less than one minute. We then used 4% paraformaldehyde to fix cells in metaphase as shown in Fig. 1. We screened the plate with a 20x water immersion objective, as oil objectives have front oil problems during stage motions preventing proper imaging. Furthermore, we also used a water dispenser (Leica) to overcome water evaporation and to ensure a perfect immersion throughout the screening. All acquired images were analysed as described previously (Fig. 4). The resulting fluorescence lifetimes are plotted as a heat map for each well (Fig. 5A, left panel). All cells within a well do not display the same number of pixels with photon count above the threshold (see analysis section). To avoid an imbalance, we weighted the lifetime from each cell by its area in pixels and the standard deviation for each cell before to calculate the mean lifetime for each well. Such a heat map showed a correct accuracy allowing to clearly distinguish between wells with GFP-AURKA and GFP-AURKA-mCherry. When pooling the fluorescence lifetimes from both conditions (Fig. 5A, right panel), we found a significant difference of about 90 ps, similar to FRET measurement in single-cell experiments (Fig. 5B).

To go further, we implemented a blind screening test on 47 molecules provided by KISSf (Roscoff). These molecules were chosen for their ability to inhibit Aurora B kinase activity by classic in vitro kinase assay. Each molecule's name referred to the well coordinates within the 96-well plate. We incubated cells expressing GFP-AURKA-mCherry with these molecules at 1 µM for 30 minutes at 37°C and fixed the cells before screening following our methodology (Fig 5.C). The results showed that several molecules were potential inhibitors of AURKA, as the fluorescence lifetime significantly increased for molecules A6, A7, D5-7, E6, G7, H5 and H6 when compared to DMSO. Interestingly, these results were strengthened by the revelation that compound H5 was MLN8237, a common inhibitor of AURKA. These results demonstrate the potentiality of our biosensor system as an automated tool for molecular screening purposes.

Conclusion

We described a method to perform automated screening with FLIM using our time-gated fastFLIM microscope. This microscope uses temporal gates to selectively acquire sections of the fluorescence decay after each pulsed laser. Our system is controlled by the Inscoper imaging suite, which allows getting rid of the latency caused by the operating system. Taking advantage of its speed, we improved it to automatically screen 96-well plates. Furthermore, we

implemented multi-well randomized acquisitions modules with an autofocus module. We also developed a pipeline to automatically analyse thousands of images and obtain fluorescence lifetime data for each cell. Importantly, the software can rapidly generate an image of fluorescence lifetime without any fitting. We validated this methodology by screening the FRET efficiency using our AURKA biosensor. We now aim to screen for novel compounds and find new and potentially more potent drugs. Furthermore, this methodology can also be used to characterize these drugs and the cellular phenotype they induce, through the fluorescence images obtained. To date, few High Content Analysis (HCA)-FLIM systems have arisen. These generate time-gated windows with a pulsed laser, but fitting to determine fluorescence lifetime is necessary (Görlitz et al., 2017) which does not permit to automate the analysis. These tools were recently used to investigate protein-protein interactions in an HCA mode (Guo et al., 2019; Margineanu et al., 2016). We here demonstrated that using biosensors and specially kinase activity biosensor increases the information that can be obtained from screening procedures. Combined to our recent multiplex systems (Demeautis et al., 2017) it will allow to track the activity of several biosensors at the same time and broaden the impact of HCA-FLIM to provide more insight into kinase activity.

Acknowledgments

We warmly thank Sandrine Ruchaud and Thomas Robert (Station Biologique de Roscoff) for providing us the library of kinase inhibitors used in this study. We acknowledge Giulia Bertolin for advice and comments during the execution of this project and for careful reading of the manuscript. We also acknowledge Sébastien Huet for fruitful discussions. We thank Stéphanie Dutertre, Clément Chevalier and Xavier Pinson of the Microscopy-Rennes Imaging Centre (Biologie, Santé, Innovation Technologique, BIOSIT, Rennes, France) for assistance. We warmly acknowledge Olivier Chanteux, Jeremy Pont and Baptiste Giroux from Inscoper providing all the necessary help in this project. We also thank Sylvain Prigent for assistance with ImageJ macros and Yann Le Cunf for sharing his expertise in data analysis. This work was supported by the Centre Nationale de la Recherche Scientifique and the Université de Rennes 1, by the Comité d'Ille et Vilaine, Comité du Maine et Loire et Comité de la Sarthe to MT, by the Infrastructures en Biologie Santé et Agronomie (IBiSA), région Bretagne and Rennes Métropole for the development of the fastFLIM prototype, and by Région Bretagne for a tech-transfer grant to MT and Inscoper. FS was supported by a PhD fellowship from Région

Bretagne and the University of Rennes1, together with an additional fellowship from the Ligue Nationale Contre le Cancer.

Competing interest

O.B. is the CTO of Inscoper Company, a spin-off of the IGDR. J.P. and M.T. are scientific advisors of Inscoper. All other authors have no competing interest.

Author contributions

F.S. designed, performed and analysed the experiments; G.L., J.P. and O.B developed tools and methods and; M.T. conceptualised the study, coordinated the work and provided funding. F.S. and M.T. wrote the paper with the input of all authors.

References

Becker, W. (2012). Fluorescence lifetime imaging – techniques and applications. Journal of Microscopy *247*, 119–136.

Bertolin, G., Sizaire, F., Herbomel, G., Reboutier, D., Prigent, C., and Tramier, M. (2016). A FRET biosensor reveals spatiotemporal activation and functions of aurora kinase A in living cells. Nature Communications *7*, 12674.

Bertolin, G., Bulteau, A.-L., Alves-Guerra, M.-C., Burel, A., Lavault, M.-T., Gavard, O., Le Bras, S., Gagné, J.-P., Poirier, G.G., Le Borgne, R., et al. (2018). Aurora kinase A localises to mitochondria to control organelle dynamics and energy production. ELife *7*, e38111.

Bischoff, J.R., Anderson, L., Zhu, Y., Mossie, K., Ng, L., Souza, B., Schryver, B., Flanagan, P., Clairvoyant, F., Ginther, C., et al. (1998). A homologue of Drosophila aurora kinase is oncogenic and amplified in human colorectal cancers. The EMBO Journal *17*, 3052–3065.

Demeautis, C., Sipieter, F., Roul, J., Chapuis, C., Padilla-Parra, S., Riquet, F.B., and Tramier, M. (2017). Multiplexing PKA and ERK1&2 kinases FRET biosensors in living cells using single excitation wavelength dual colour FLIM. Scientific Reports *7*, 41026.

Glover, D.M., Leibowitz, M.H., McLean, D.A., and Parry, H. (1995). Mutations in aurora prevent centrosome separation leading to the formation of monopolar spindles. Cell *81*, 95–105.

Görlitz, F., Kelly, D.J., Warren, S.C., Alibhai, D., West, L., Kumar, S., Alexandrov, Y., Munro, I., Garcia, E., McGinty, J., et al. (2017). Open Source High Content Analysis Utilizing Automated Fluorescence Lifetime Imaging Microscopy. JoVE 55119.

Guo, W., Kumar, S., Görlitz, F., Garcia, E., Alexandrov, Y., Munro, I., Kelly, D.J., Warren, S., Thorpe, P., Dunsby, C., et al. (2019). Automated Fluorescence Lifetime Imaging High-Content Analysis of Förster Resonance Energy Transfer between Endogenously Labeled Kinetochore

Proteins in Live Budding Yeast Cells. SLAS TECHNOLOGY: Translating Life Sciences Innovation 247263031881924.

Guzmán, C., Oetken-Lindholm, C., and Abankwa, D. (2016). Automated High-Throughput Fluorescence Lifetime Imaging Microscopy to Detect Protein-Protein Interactions. J Lab Autom *21*, 238–245.

Hochreiter, B., Garcia, A., and Schmid, J. (2015). Fluorescent Proteins as Genetically Encoded FRET Biosensors in Life Sciences. Sensors *15*, 26281–26314.

Horton, R.A., Strachan, E.A., Vogel, K.W., and Riddle, S.M. (2007). A substrate for deubiquitinating enzymes based on time-resolved fluorescence resonance energy transfer between terbium and yellow fluorescent protein. Analytical Biochemistry *360*, 138–143.

Kenworthy, A.K. (2001). Imaging Protein-Protein Interactions Using Fluorescence Resonance Energy Transfer Microscopy. Methods *24*, 289–296.

Lakowicz, J.R. (2006). Principles of Fluorescence Spectroscopy (Springer US).

Leray, A., Padilla-Parra, S., Roul, J., Héliot, L., and Tramier, M. (2013). Spatio-Temporal Quantification of FRET in Living Cells by Fast Time-Domain FLIM: A Comparative Study of Non-Fitting Methods. PLoS ONE *8*, e69335.

Liu, W., Cui, Y., Ren, W., and Irudayaraj, J. (2019). Epigenetic biomarker screening by FLIM-FRET for combination therapy in ER+ breast cancer. Clinical Epigenetics *11*.

Margineanu, A., Chan, J.J., Kelly, D.J., Warren, S.C., Flatters, D., Kumar, S., Katan, M., Dunsby, C.W., and French, P.M.W. (2016). Screening for protein-protein interactions using Förster resonance energy transfer (FRET) and fluorescence lifetime imaging microscopy (FLIM). Scientific Reports *6*.

Miyawaki, A., Llopis, J., Heim, R., McCaffery, J.M., and others (1997). Fluorescent indicators for Ca2+ based on green fluorescent proteins and calmodulin. Nature *388*, 882.

Nikonova, A.S., Astsaturov, I., Serebriiskii, I.G., Dunbrack, R.L., and Golemis, E.A. (2013). Aurora A kinase (AURKA) in normal and pathological cell division. Cellular and Molecular Life Sciences *70*, 661–687.

Padilla-Parra, S., and Tramier, M. (2012). FRET microscopy in the living cell: Different approaches, strengths and weaknesses. BioEssays *34*, 369–376.

Qiu, Y., Chen, X., Li, Y., Chen, W.R., Zheng, B., Li, S., and Liu, H. (2013). Evaluations of Auto-Focusing Methods under a Microscopic Imaging Modality for Metaphase Chromosome Image Analysis. Analytical Cellular Pathology *36*, 37–44.

Richert, L., Didier, P., de Rocquigny, H., and Mély, Y. (2015). Monitoring HIV-1 Protein Oligomerization by FLIM FRET Microscopy. In Advanced Time-Correlated Single Photon Counting Applications, W. Becker, ed. (Cham: Springer International Publishing), pp. 277–307.

Roul, J., Tramier, M., and Pecreaux, J. (2015). Method for controlling a plurality of functional modules including a multi-wavelength imaging device, and corresponding control system.

Sen, S., Zhou, H., and White, R.A. (1997). A putative serine/threonine kinase encoding gene BTAK on chromosome 20q13 is amplified and overexpressed in human breast cancer cell lines. Oncogene *14*, 2195–2200.

Sizaire, F., and Tramier, M. (2017). FRET-Based Biosensors: Genetically Encoded Tools to Track Kinase Activity in Living Cells. IntechOpen *Protein Phosphorylation*.

Thomas, N. (2010). High-Content Screening: A Decade of Evolution. Journal of Biomolecular Screening *15*, 1–9.

Zhang, J., Ma, Y., Taylor, S.S., and Tsien, R.Y. (2001). Genetically encoded reporters of protein kinase A activity reveal impact of substrate tethering. Proceedings of the National Academy of Sciences *98*, 14997–15002.

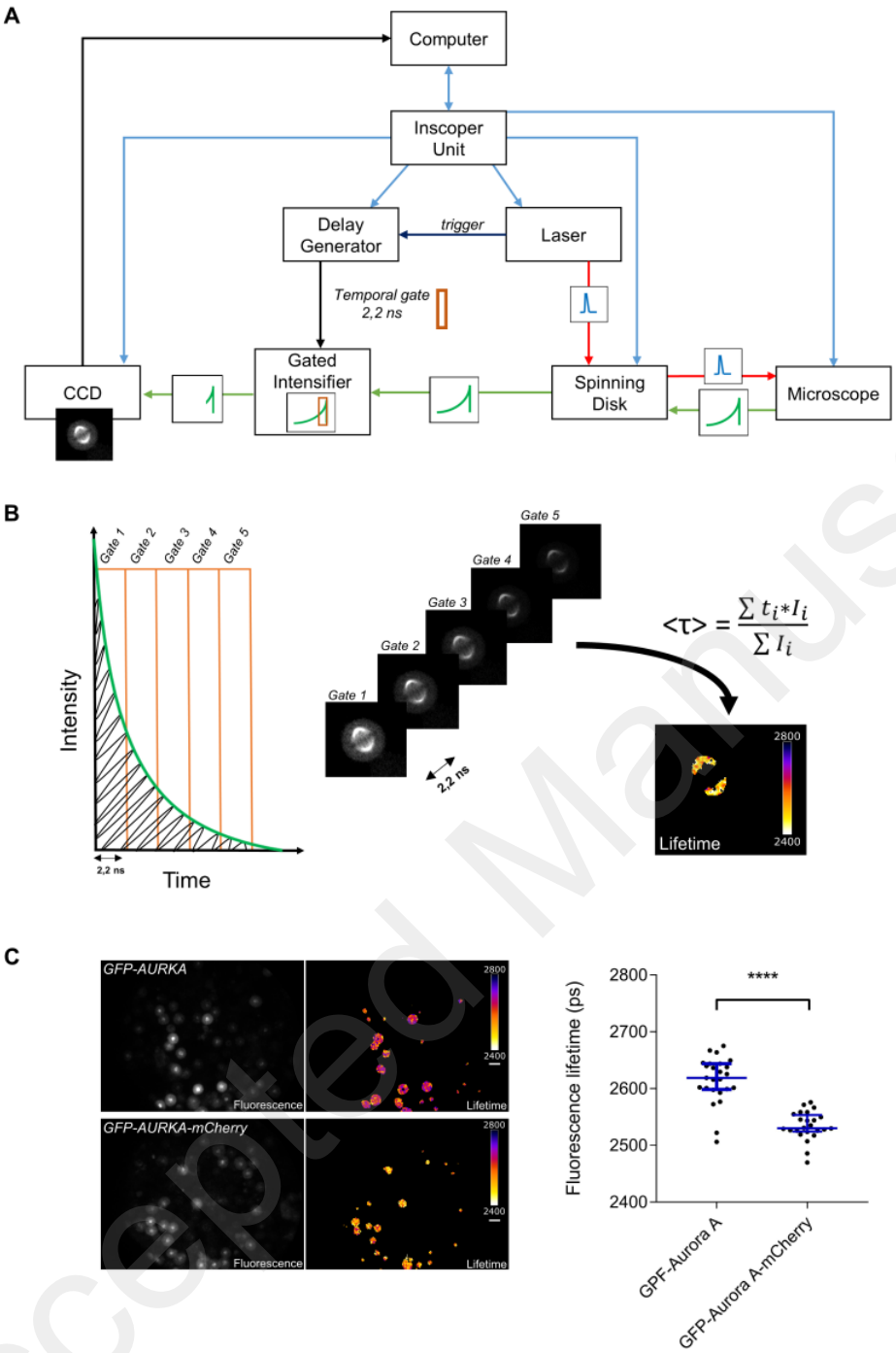

Fig. 1. The fast-FLIM microscope can measure FRET efficiency of the AURKA biosensor in fixed cell lines. **A.** Model illustrating the mode of action of the fast-FLIM. The computer sends commands to the Inscoper electronic unit, which in turn communicates with the other devices. For each laser pulse, a trigger from the laser is sent to the, intensifier generating a gate of 2.2 ns during which the fluorescence emission is captured. The delay generator is used to position the gate at the desired timing during the fluorescence decay. After intensifying the fluorescence signal of the selected temporal gate, a CCD camera is used to acquire the time-

gated image and is sent to the computer. **B.** Model illustrating the generation of one fluorescence lifetime image using the AURKA biosensor in U2OS cells. A stack of fives time-gated images are acquired sequentially after controlling the delay generator to position the gate. Each image corresponds to a juxtaposed gate of 2.2 ns to cover the whole fluorescence decay. From the intensity of the five images, the pixel by pixel mean fluorescence lifetime is calculated using a discrete temporal mean of the decay to form the fluorescence lifetime image. **C.** The fast-FLIM is suitable to measure FRET efficiency of the AURKA biosensor in fixed cells. (Left panel) On the left, representative fluorescence (GFP channel) of U2OS cells expressing GFP-AURKA or GFP-AURKA-mCherry, synchronized at mitosis, fixed with 4% paraformaldehyde and imaged with a 20x objective (NA = 0.7). On the right, the corresponding fluorescence lifetime images. Pseudocolour scale correspond to the mean lifetime. Scale bar, 30 µm. (Right panel) Corresponding scatter plot of the fluorescence lifetime; Each dot corresponds to the fluorescence lifetime of one cell. n=20-30 cells per condition from three independent experiments.Blue bars represent median and interquartile. ***P<0.0001 against the 'GFP-AURKA' condition. Statistical test: Wilcoxon-Mann-Whitney test.

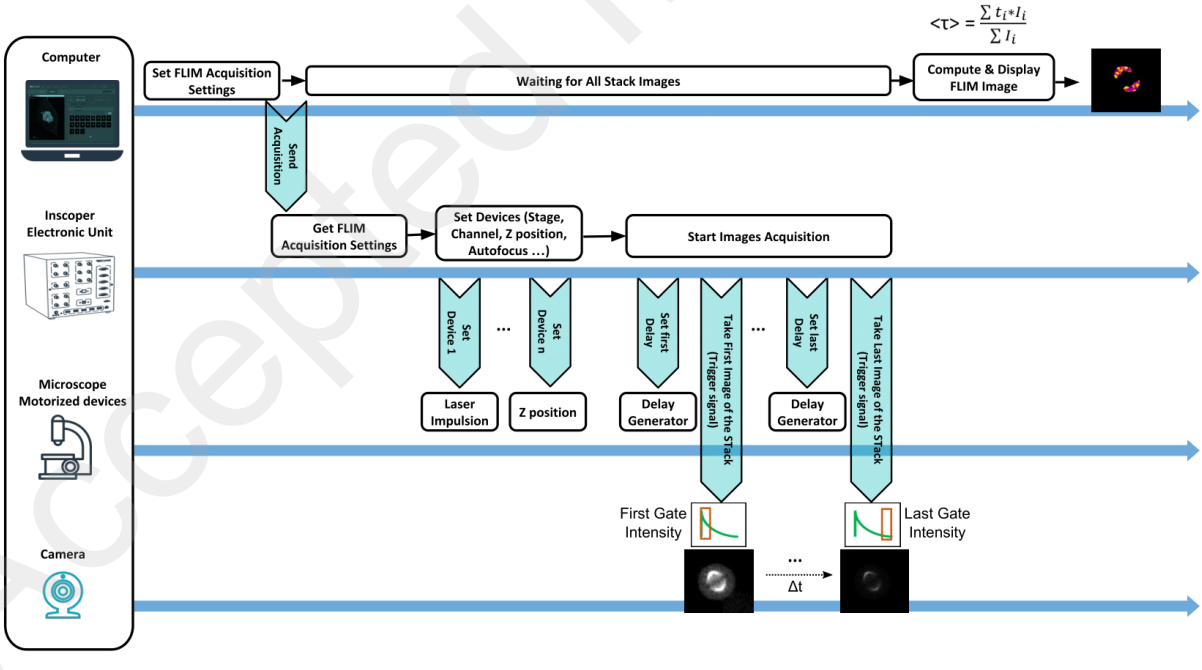

Fig. 2. Hardware and Software features for the acquisition of a FLIM image. From right to left and from top to bottom: from the Inscoper graphical user interface on the computer, the user set FLIM acquisition sequence which is sent to the Inscoper electronic unit. While computer wait for the acquired images, the Inscoper unit analyses the sequence parameters and

set the different devices by communicating to the different microscope devices. Then the electronic unit starts the acquisition of the stack of time-gated images by alternatively setting thee delay generator and triggering the camera. All the camera images where then transferred to the computer and when the stack is completed, the computer calculate and display the FLIM image. In the same time, the Inscoper electronic unit re-start a new FLIM acquisition after setting the different devices if necessary as it was previously planned by the user at the beginning of the acquisition sequence. The process is reproduced as many times as necessary to complete the full sequence.

A

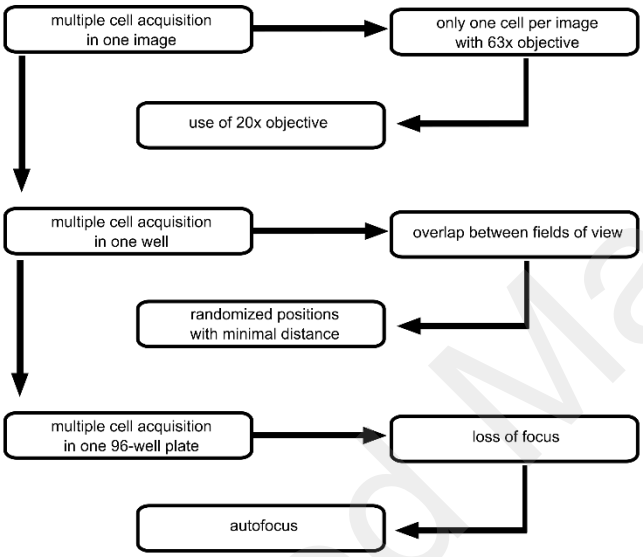

B

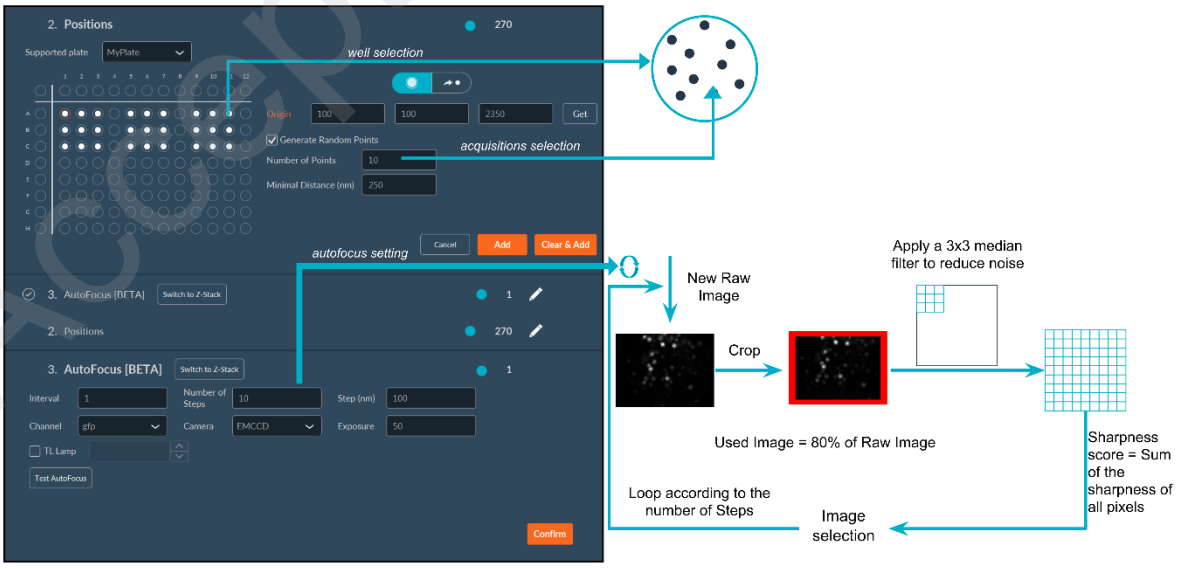

Fig3. Multi-well and autofocus modules of the Inscoper user interface for screening applications. **A.** Workflow diagram of the screening strategy. **B.** Inscoper User Interface. At the top left of the windows is presented the scheme of the 96 multi-well plates. The user determines the wells of interest (where the acquisition will be carried out) by individual well, by line or by column. Then the user determines the number of random points for each well and the minimum distance between each position (as presented in the scheme at the top right). With these information, the interface calculates the coordinates of each point based on the initial calibration of the stage. At the bottom of the windows is presented the autofocus panel which permits to determine the optimal z plane for each xy position. The user determines the interval, the number of steps, the step size and the color channel used for autofocus. The algorithm then calculates the best focus by calculating a sharpness score for each acquired image (see Results section for details). The plan with the highest score is selected. To speed up the execution of the autofocus, it is possible to define a dedicated exposure time different to the FLIM images.

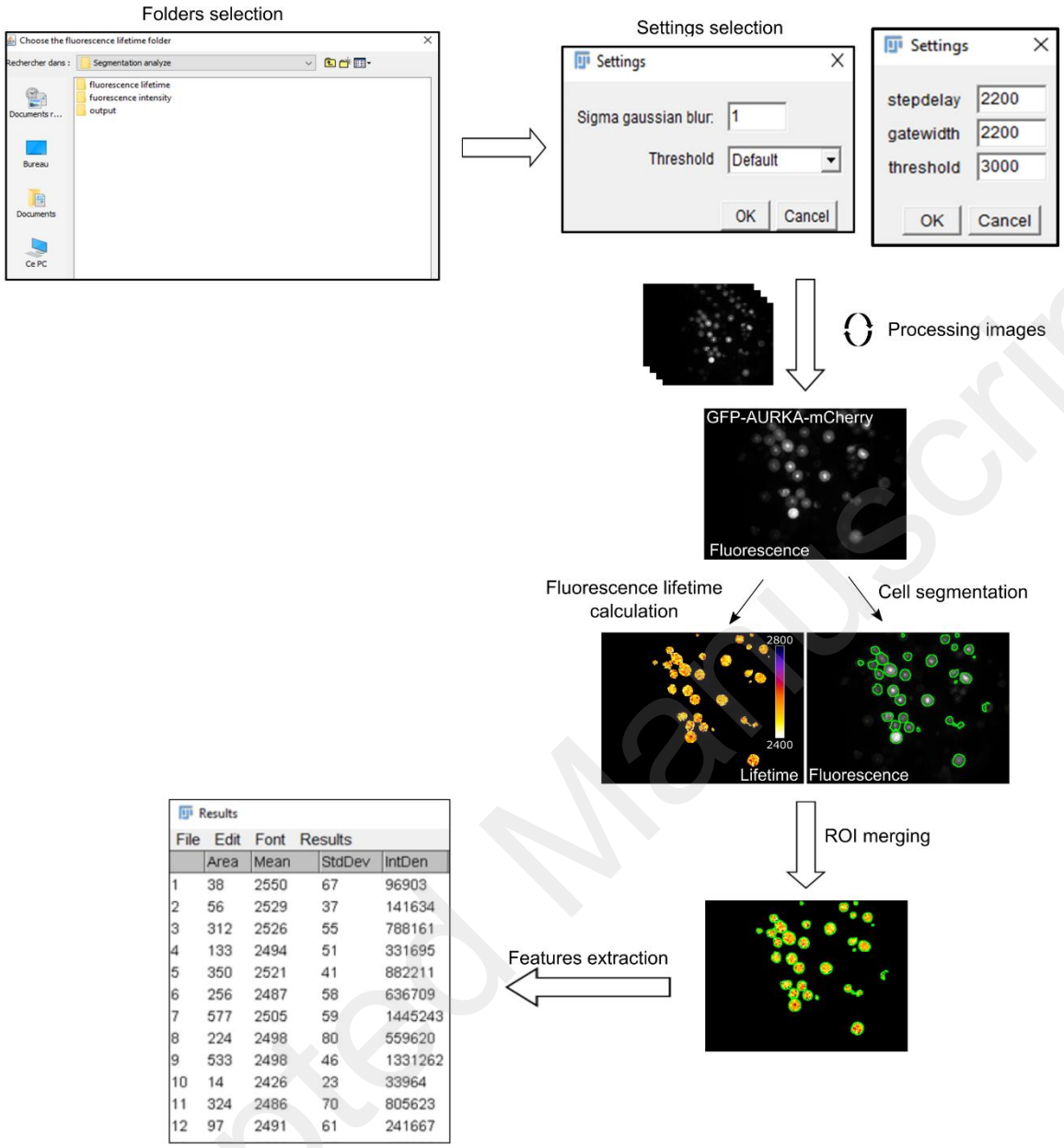

	Area	Mean	StdDev	IntDen
1	38	2550	67	96903
2	56	2529	37	141634
3	312	2526	55	788161
4	133	2494	51	331695
5	350	2521	41	882211
6	256	2487	58	636709
7	577	2505	59	1445243
8	224	2498	80	559620
9	533	2498	46	1331262
10	14	2426	23	33964
11	324	2486	70	805623
12	97	2491	61	241667

Fig. 4. Batch mode analysis by cell segmentation. Analysis of fluorescence images of U2OS expressing GFP-AURKA-mCherry using an ImageJ home-made macro. From top to bottom: the user first chooses the folder containing fluorescence images, and the two destination folders for the calculated lifetime image and for the segmented intensity images with a file containing all the values of the features for each ROI. From the stack of time-gated images, the fluorescence lifetime image is generated using the threshold, size of the gate and step values settled by the user. From the first time-gated fluorescence image, the cells are segmented according to the settings defined by the user. This segmentation is applied on the fluorescence lifetime image and for each ROI (cell) is calculated the mean fluorescence lifetime, the number

of pixel (area of the ROI) and the standard deviation between the pixel values. This analysis is automatically applied for all the images coming from the chosen folder.

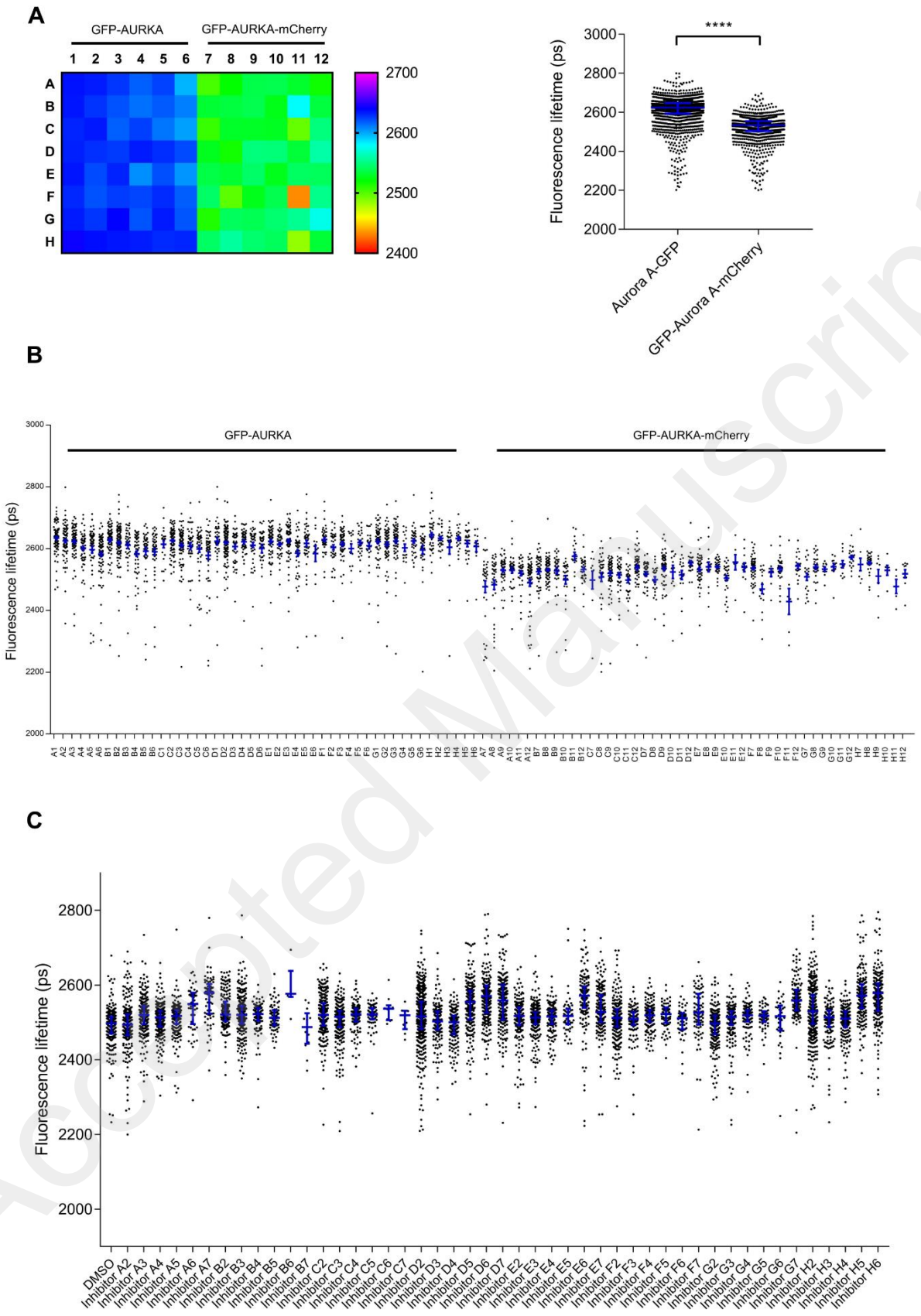

Fig 5. Multiwell plate screening of AURKA biosensor. A. (Left panel) Heatmap of the mean fluorescence lifetime values weighted by the area and the standard deviation in each well of a

96-well plate seeded with U2OS cells expressing GFP-AURKA and GFP-AURKA-mCherry. Cells have been synchronized at mitosis and fixed with PFA before being screened with the HCS-FLIM. Pseudocolour scale: lifetime values in ps. (Right panel) Corresponding scatter plot of the fluorescence lifetime values coming from all the wells expressing GFP-AURKA or GFP-AURKA-mCherry. Each dot represents lifetime of one cell and blue bars represent median and interquartile.. ****P<0.0001 against the GFP-AURKA condition. Statistical test: Wilcoxon-Mann-Whitney test. **B.** Scatter plot of fluorescence lifetime values of each cell sorted by well (from A1 to H12). Each individual point represents a single cell. Bars represent median and interquartile. **C.** Scatter plot of fluorescence lifetime values of each cell sorted by inhibitor treatment. Each individual point represents a single cell. Bar represent median and interquartile.